Interpreting the dependence of cloud-radiative adjustment on forcing agent

Article

Salvi, Pietro, Ceppi, Paulo and Gregory, Jonathan M. (2021) Interpreting the dependence of cloud-radiative adjustment on forcing agent. Geophysical Research Letters, 48 (18). e2021GL093616. ISSN 0094-8276 doi: https://doi.org/10.1029/2021GL093616 Available at https://centaur.reading.ac.uk/99940/

www.reading.ac.uk/centaur

CentAUR

Central Archive at the University of Reading

Interpreting the Dependence of Cloud-Radiative Adjustment on Forcing Agent

Pietro Salvi[1] , **Paulo Ceppi[1]** , and **Jonathan M. Gregory[2,3]**

[1]Department of Physics & Grantham Institute, Imperial College London, London, UK, [2]National Centre for Atmospheric Science, University of Reading, Reading, UK, [3]Met Office Hadley Centre, Exeter, UK

Abstract Effective radiative forcing includes a contribution by rapid adjustments, that is, changes in temperature, water vapor, and clouds that modify the energy budget. Cloud adjustments in particular have been shown to depend strongly on forcing agent. We perform idealized atmospheric heating experiments to demonstrate a relationship between cloud adjustment and the vertical profile of imposed radiative heating: boundary-layer heating causes a positive cloud adjustment (a net downward radiative anomaly), while free-tropospheric heating yields a negative adjustment. This dependence is dominated by the shortwave effect of changes in low clouds. Much of the variation in cloud adjustment among common forcing agents such as CO_2, CH_4, solar forcing, and black carbon is explained by the "characteristic altitude" (i.e., the vertical center-of-mass) of their heating profiles, through its effect on tropospheric stability.

Plain Language Summary Changes in factors such as greenhouse gas concentrations or solar irradiance affect the balance of energy coming into versus leaving the earth's atmosphere, a phenomenon known as radiative forcing. This forcing can be modified by rapid atmospheric "adjustments" that occur in temperature, humidity, and cloud cover. The cloud component in particular of these rapid adjustments strongly depends on the forcing agent, for reasons that have been unclear. We find that the vertical structure of atmospheric heating explains much of the forcing agent dependence of the cloud adjustments: bottom-heavier heating causes a more positive cloud adjustment. By understanding what happens when only a small portion of the atmosphere is heated, we show that it is possible to explain cloud adjustments to more complex forcings. We anticipate that our results will provide a physical basis to understand the causes of model-to-model differences in cloud adjustments.

1. Introduction

Radiative forcing quantifies the perturbation to the Earth's energy budget associated with a particular climatic factor, such as greenhouse gases, aerosols, or solar irradiance. Forcing was originally defined as the instantaneous perturbation to the Earth's radiative budget due to the forcing agent. Later, the concept was refined to include the effect on the tropospheric heat budget of stratospheric adjustment due to radiative changes, which are particularly important for carbon dioxide (K. Shine et al., 1995). More recently, "effective radiative forcing" (ERF) has become the usual metric (Myhre et al., 2014), which additionally accounts for relatively short-timescale tropospheric adjustments in temperature, moisture, and clouds that are direct responses to the forcing, rather than being mediated by surface warming (Andrews & Forster, 2008; Gregory & Webb, 2008; Sherwood et al., 2015). This approach is justified by the fact that ERF is a better predictor of the surface temperature response than instantaneous radiative forcing (IRF) (Richardson et al., 2019) or stratosphere-adjusted forcing (K. P. Shine et al., 2003).

The rapid adjustments to radiative forcing have been found to make a substantial contribution to model uncertainty in ERF for a variety of forcing agents including anthropogenic greenhouse gases, aerosols and solar irradiance (Chung & Soden, 2015; Smith et al., 2018, 2020). Cloud adjustments account for a large part of these differences (Andrews et al., 2012; Colman & McAvaney, 2011; Smith et al., 2018; Zelinka et al., 2013), consistent with clouds being an important source of uncertainty in the response to forcing among climate models (Ceppi et al., 2017), especially in the case of aerosols. Aerosol-*radiation* interactions lead to cloud adjustments (known as semi-direct effects) by modifying local atmospheric conditions. Aerosol-*cloud* interactions lead to further cloud adjustments via microphysical changes (known as indirect

effects; Bellouin et al., 2020). Only the cloud adjustments due to semi-direct effects will be considered in this paper.

Several past papers have investigated the mechanisms of cloud adjustments in response to CO_2 forcing (e.g., Dinh & Fueglistaler, 2017; Kamae & Watanabe, 2012, 2013; Kamae et al., 2015, 2019; Zelinka et al., 2013) and to absorbing aerosols such as black carbon (BC) (Ban-Weiss et al., 2012; Bellouin et al., 2020; Koch & Del Genio, 2010; Samset & Myhre, 2015; Sand et al., 2020; Stjern et al., 2020) or dust (Amiri-Farahani et al., 2017), but there is a lack of process studies involving other forcing agents. Smith et al. (2018) demonstrated a striking forcing agent dependence of cloud adjustments across Coupled Model Intercomparison Project phase 5 (CMIP5) models, with consistently positive adjustments to CO_2 and negative adjustments to solar and BC forcing (we define downward radiative anomalies at the top of atmosphere as positive). However, there is currently limited understanding of how different cloud adjustments arise in response to various instantaneous forcings.

In this study, we address this knowledge gap by interpreting the forcing agent dependence of cloud adjustment in terms of the spatial structure of instantaneous atmospheric forcing. Specifically, we propose here that the vertical profile of atmospheric heating is a key factor for this forcing agent dependence. For absorbing aerosols, previous studies have identified a dependence of semi-direct cloud adjustments upon forcing altitude: typically positive for boundary-layer forcing, negative for free-tropospheric forcing (Amiri-Farahani et al., 2017; Ban-Weiss et al., 2012; Bellouin et al., 2020; Koch & Del Genio, 2010; Samset & Myhre, 2015; Stjern et al., 2020). Here we expand on these previous works to show that the vertical heating profile explains much of the cloud adjustment in response to a diverse range of forcing agents. This is demonstrated through comparison of idealized and common forcing experiments with a CMIP5-class climate model.

2. Data and Methods

The simulations used for this paper were run with the CAM4 model (Neale et al., 2010) in an atmosphere-only configuration with prescribed sea surface temperatures (SSTs) and sea ice concentrations. A $1.9° \times 2.5°$ latitude/longitude grid was used with 26 vertical levels. Simulations were run for 20 years with the climatology calculated as the average of monthly mean data output from the model for all but the first simulated year, during which the atmosphere was adjusting to reach a steady state in the presence of the forcing. The vertical profiles shown in this paper were linearly interpolated from the model's 26 hybrid sigma-pressure levels to a 100-level pure pressure grid so as to allow for averaging along pressure levels. This was done using evenly spaced levels between 0 and 1,000 hPa.

Instantaneous and ERFs were calculated for four forcing agents: a 10-fold increase in methane ($10 \times CH_4$), doubled carbon dioxide ($2 \times CO_2$), a 10-fold increase in black carbon ($10 \times BC$), and a 3% increase to incoming solar radiation (3%Sol) (see Table S1). These are among the forcing agents as used in the Precipitation Driver Response Model Intercomparison Project (PDRMIP) set of experiments (Myhre et al., 2017), although not all with the same magnitudes as in the PDRMIP experiments. IRF was calculated using the Parallel Offline Radiative Transfer tool for CAM4, by taking the difference between perturbed and control instantaneous radiative fluxes (Conley et al., 2013). For these fluxes, simulations were run for 18 months starting on January 1st with outputs every 73 time steps (roughly 1.5 days) as recommended by Conley et al. (2013). The fluxes used were the averages over the last 12 months of these simulations. To obtain the ERF, the difference in mean climate was taken between perturbed and control CAM4 experiments with SSTs and sea ice fixed to the control state (Hansen et al., 1997). Note that the CO_2 concentration was doubled only in the radiation scheme in the $2 \times CO_2$ experiment, so the model did not simulate a plant physiological response to CO_2, which has been found to cause significant cloud-radiative adjustments (Doutriaux-Boucher et al., 2009). Furthermore, CAM4 does not simulate aerosol-cloud interactions for black carbon, whose atmospheric concentrations are prescribed.

In addition to the common forcing cases (Table S1), experiments were also performed with idealized, horizontally homogeneous forcings (Table S2), prescribed as an extra heating rate in CAM4's radiation scheme. This includes a uniform surface heating (sfc_4) of 4 W m^{-2}, and a vertically and horizontally uniform atmospheric heating (atm_4) whose vertical integral is 4 W m^{-2}. Furthermore, we also apply vertically localized

heating anomalies at specific atmospheric levels ϕ (vloc_ϕhPa; Figure S1). The applied heating rate anomalies for the vloc_ϕhPa forcing experiments were defined as follows:

$$
\begin{aligned}
\Delta Q(p) &= A\cos^2\left(\frac{(p-\phi)\pi}{2a}\right) \quad \text{for } (\phi - a) \le p \le (\phi + a) \\
\Delta Q(p) &= 0 \qquad\qquad\qquad\quad \text{otherwise}
\end{aligned}
\tag{1}
$$

for pressure p and heating centered at ϕ, where $A = \pm 0.135\,\text{K day}^{-1}$, $a = 125\,\text{hPa}$, and ΔQ is the instantaneous atmospheric heating anomaly from the control. This provides a vertically integrated heating of $2\,\text{W m}^{-2}$, except for the topmost and lowermost vertically localized experiments which are truncated at the pressure limits (Figure S1) and thus provide around half the vertically integrated forcing. The whole atmosphere was covered by nine of these bounded $\cos^2$ heating profiles centered on multiples of 125 hPa between 0 and 1,000 hPa (inclusive). The $\cos^2$ shape combined with the $2a$ heating profile widths mean that the sum of these profiles is uniform in pressure. The width a was chosen such that the forcings are sufficiently localized in the vertical, while still being adequately resolved by CAM4's vertical grid. To test the linearity of the responses, both positive and negative vertically localized heating tendencies were applied.

Similar approaches of attempting to understand responses to complex spatial forcing by looking at linear combinations of individual localized forcings have appeared several times in the literature (Beucler et al., 2018; Dong et al., 2019; Kuang, 2010; Zhou et al., 2017). Past studies have also investigated energy input at different vertical layers by insertion of aerosol (e.g., Samset & Myhre, 2015; Sand et al., 2020). We use our experiments with various horizontally uniform heating rates to study the effect of the vertical profile of forcing.

Rather than calculating cloud adjustments as differences in cloud-radiative effect (CRE), we use cloud kernels from Zelinka et al. (2012) (see Figure S2). Unlike CRE differences, which are affected by noncloud adjustments (in temperature, water vapor, or surface albedo), the kernels quantify the radiative impact of cloud adjustment in isolation. These kernels represent partial derivatives of top of the atmosphere CRE with respect to cloud fraction changes, as a function of cloud top pressure (CTP) and optical depth. They thus allow the radiative adjustments to be broken down into contributions from high (CTP < 440 hPa), mid (440 < CTP < 680 hPa), and low (CTP > 680 hPa) clouds. To use the cloud kernels, the International Satellite Cloud Climatology Project (ISCCP) satellite simulator (Swales et al., 2018) was enabled in CAM4 to output the required cloud fraction histograms (see Figure S2 for an example).

We introduce two measures in this paper to help understand the relationship between the vertical profile of atmospheric forcing, tropospheric stability, and cloud-radiative adjustment. First, to characterize the vertical distribution of forcing $Q(p)$, we define a "heating-weighted pressure centroid":

$$
\frac{\int_{p=200\text{hPa}}^{1,000\text{hPa}} p \cdot Q(p)\,dp}{\int_{p=200\text{hPa}}^{1,000\text{hPa}} Q(p)\,dp}
\tag{2}
$$

This is understood as the "center-of-mass" of the forcing, defined such that larger values here denote a bottom-heavier atmospheric forcing profile. Note that the pressure centroid is positive for the vertically localized heating tendencies of either sign. In general, the pressure centroid is positive and readily interpreted for atmospheric forcings which are entirely or mostly of the same sign at all pressures, as is the case for all those we consider.

Second, for tropospheric stability, we define the "bulk tropospheric stability" (BTS) as the difference between the average potential temperature (Θ) for the 200–800 hPa layer ($\Theta_{200-800}$), taken as representative of the free troposphere, and $\Theta_{800-1,000}$, taken as representative of the boundary layer:

$$
\text{BTS} = \Theta_{200-800} - \Theta_{800-1,000}.
\tag{3}
$$

3. Vertically Localized Atmospheric Heating Experiments

To gain insight into the dependence of cloud adjustments on forcing altitude, we begin with the results from the vertically localized forcing experiments. Focusing on the vertical structure, Figure 1 shows the global-mean adjustments of temperature (T), relative humidity (RH), and cloud fraction for three of the vertically localized forcings (chosen as examples). A close correspondence is found between the peak of
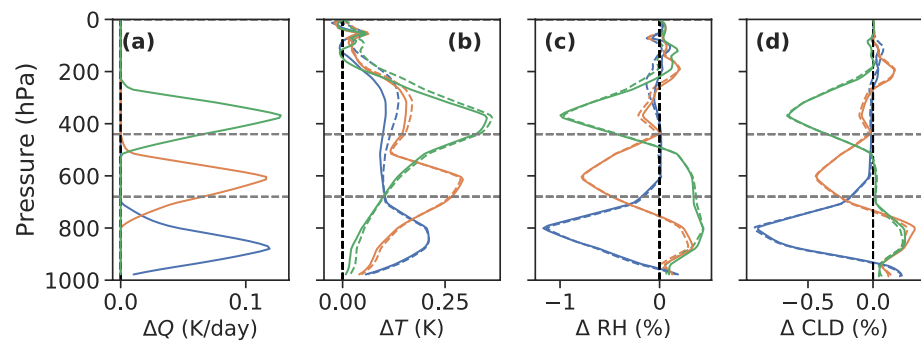
Figure 1. Profiles for (a) applied heating rates ΔQ, as well as (b) temperature, (c) relative humidity (RH), and (d) cloud fraction (CLD) change profiles for vertically localized heating experiments with ϕ = 875 hPa (*blue*), ϕ = 625 hPa (*orange*), and ϕ = 375 hPa (*green*). Profiles shown in solid lines are the average of the positive and negative of the negative vertically localized heating tendencies set at the same heights and magnitudes. The profiles for the heating experiments are shown separately as dashed lines. Heating profiles are interpolated from model input, rather than those defined in Equation 1. The gray horizontal lines demarcate bounds between high, mid, and low levels according to the International Satellite Cloud Climatology Project simulator. Changes to temperature, RH, and cloud are obtained as the difference between the equilibrium fixed sea surface temperature state and a control state.

applied heating and the peaks of changes to *T* and RH, as well as cloud fraction. Furthermore, there is a striking similarity between the profiles of changes to RH and cloud fraction, as expected.

Increased temperature without significant specific humidity changes results in RH reductions that are associated with cloud reductions. Additionally, however, the vertically localized forcings also cause nonlocal changes via changes in stratification and their impacts on vertical heat and moisture fluxes. Heating at lower levels (in the boundary layer) destabilizes the overlying free troposphere, leading to enhanced convection and vertical mixing and resulting in warming at higher levels, but little change in RH or cloud (Figure 1, blue curves). By contrast, free-tropospheric heating causes suppressed convection at lower levels through increased tropospheric stability (Figure 2a, open symbols indicate greater positive ΔBTS for vertically localized heating at lower pressure, which means higher altitude), leading to increases to RH and cloud fraction at lower levels (Figure 1, orange and green curves).

In the tropics, low cloud changes occur predominantly in subsidence regions with only small changes in regions of ascent such as the Indo-Pacific warm pool (Figures S3a and S3b), whereas changes to high cloud are more evenly distributed (panels c and d). Despite locally substantial high-cloud changes (Figure S3c), there is no global-average change in high cloud in the low tropospheric forcing scenario (Figure 2d, blue curve). This may be because slight dynamical shifts in the regions of ascent and descent cause local changes which cancel out spatially.

In summary, cloud fraction decreases in response to localized heating at all levels and associated drying, but low-level cloud increases in response to heating at higher levels. The latter is consistent with the known dependence of low clouds on tropospheric stability (Klein & Hartmann, 1993). Generally, these results are consistent with those from Samset and Myhre (2015, their Figure 5) and Sand et al. (2020, their Figure 6) involving application of localized BC at different atmospheric levels.

There is a strong dependence of the cloud-radiative adjustments on the altitude of applied forcing and the associated stability changes. The net cloud adjustments in Figure 2d are of substantial magnitude relative to the imposed vertically localized heating anomalies of 2 W m^{-2}—ranging from about −50% to +20% of these. This illustrates how cloud adjustments can substantially enhance or offset the instantaneous forcing, depending on the vertical distribution of anomalous heating. The cloud-radiative adjustment becomes monotonically more negative with the height of the applied heating (Figures 2c and 2d). This trend is driven by both LW and SW changes, with the latter dominating, qualitatively consistent with previous findings for BC forcing applied at different altitudes (Samset & Myhre, 2015, their Figure 1; Sand et al., 2020, their Figure 2). SW cloud adjustments flip sign from positive to negative as forcing altitude increases, while LW cloud adjustments become strongly negative (Figure 2d). The dependence of LW cloud adjustment on forcing
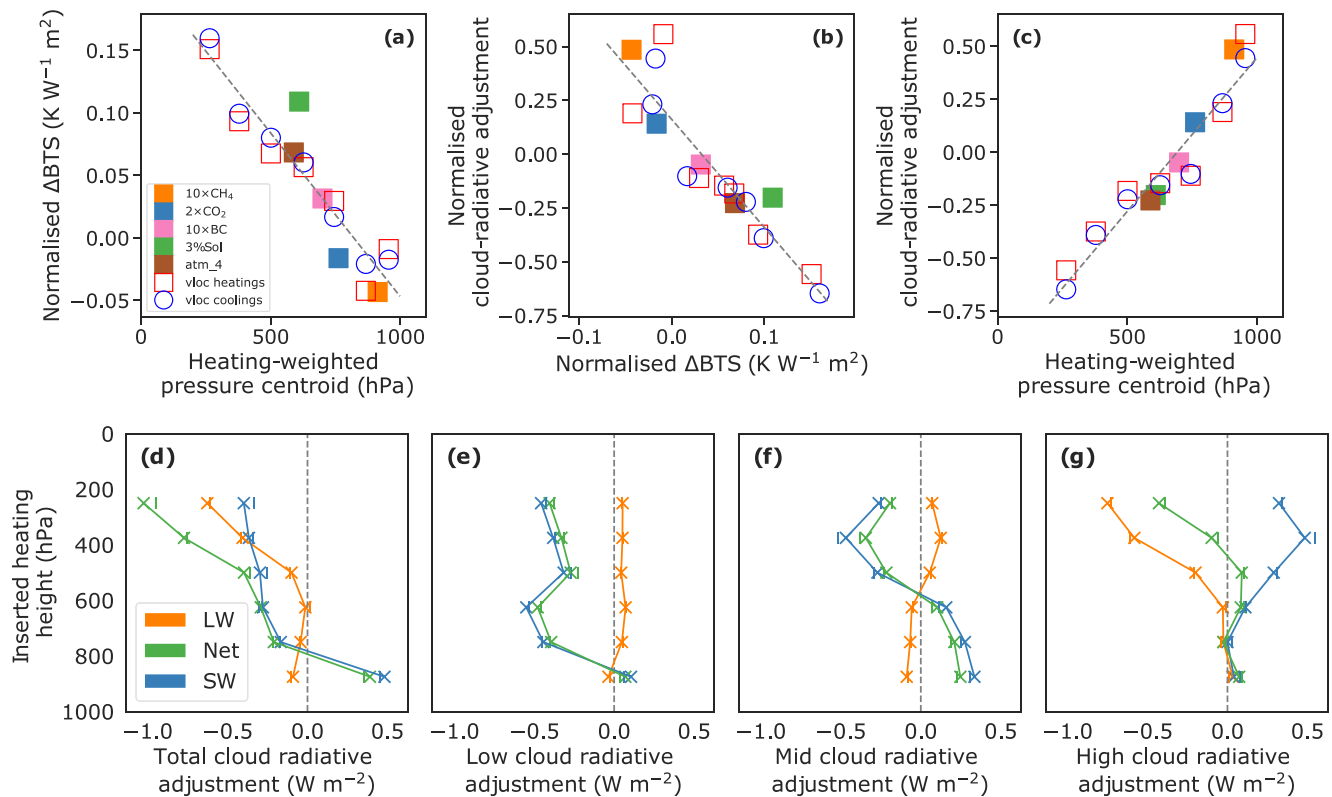
Figure 2. (a) Changes to bulk tropospheric stability (BTS, see Equation 3), normalized by the vertically integrated tropospheric (200–1,000 hPa) heating anomalies, versus the vertical center-of-mass of tropospheric heating (Equation 2) for each experiment performed in this study. (b) Normalized cloud-radiative adjustments against normalized BTS changes. (c) Normalized cloud-radiative adjustments versus heating center of mass. Least-squares linear fits are shown by the dashed lines. Only experiments with significant tropospheric forcing are shown, which excludes the 0 and 125 hPa forcing experiments. (d) Cloud-radiative adjustments from the six vertically localized forcings centered between 875 and 250 hPa, in 125-hPa increments, broken down into contributions from low (e), mid-level (f), and high (g) cloud changes. The lowest altitude forcing at 1,000 hPa is excluded because it is truncated; furthermore, the two highest altitude forcings are excluded because they are mainly in the stratosphere, and have little impact on clouds. Crosses represent the averages between the responses to heating anomalies and the negative of the responses to cooling anomalies at the same altitudes and of the same magnitudes, with the thin horizontal lines around the crosses representing the results from the heating experiments.

altitude is consistent with the understanding that LW CRE increases with cloud altitude (Hartmann, 1994), due to increased temperature differences between higher clouds and the surface.

To interpret the dependence of SW cloud adjustment on forcing altitude (Figure 2d), it is helpful to consider the breakdown of the adjustments into contributions by high-, mid- and low-level clouds (Figures 2e–2g). Low- and medium-cloud-radiative adjustments tend to be negative below the level of the heating, and positive above, while the high-cloud-radiative adjustment is negative for the highest altitude heating. All levels tend to give a negative cloud-radiative adjustment below the level of heating, while mid-level cloud contributes positively above the level of heating as well. This is consistent with the findings from Figure 1: localized heating causes a cloud fraction reduction locally, but a cloud fraction increase below (particularly in the boundary layer), associated with stabilization (Figure 2, open symbols) and suppressed vertical mixing. There is an additional factor contributing to the negative SW cloud adjustment below the vertically localized heating: when cloud fraction decreases at the heating level, the reduced overlap reveals and hence increases SW reflection from lower-level clouds.

Geographically, the radiative changes mirror the high-cloud changes in the LW (Figures S3g and S3h), spatially canceling out for the boundary layer forcing case. By contrast, the SW changes (Figures S3i and S3j) are more closely related to the changes in total cloud amount (Figures S3e and S3f) and cannot be easily attributed to a particular region or cloud regime.

We note that in Figures 1b–1d, the corresponding dashed and solid lines are similar, and in Figures 2d–2g, the corresponding crosses and vertical lines are close together. Differences are minor even in the upper troposphere, where the differences are largest. Both thus provide evidence that positive and negative heating tendencies of the same magnitude produce responses of the same magnitude and opposite sign.

Cloud adjustments are caused also by heating at the surface, but the sfc_4 experiment shows that they are very small, at all altitudes and in both LW and SW (not shown), with a net CRE adjustment of $-0.03 \, \text{W m}^{-2}$. This is negligible in comparison to the adjustments for the localized atmospheric heating experiments, especially per unit of forcing. This result is expected given the fixed-SST lower boundary, where surface forcing can impact the atmosphere only over land and ice regions. Note that although the rapid climate response to land warming under fixed SSTs is typically included in the ERF as part of the rapid adjustment (Forster et al., 2016; Sherwood et al., 2015), conceptually this can also be treated as a surface warming–driven radiative response (Chung & Soden, 2015; K. P. Shine et al., 2003).

4. Interpreting Cloud-Radiative Adjustments to Common Forcing Agents

This section seeks to explain adjustments to some common forcing agents (Table S1) in light of the findings of Section 3 concerning vertically localized heating. For each of the common forcings (as well as the idealized atm_4 case), we express the vertical profile of global-mean heating as a linear combination of idealized vertically localized heating perturbations:

$$\Delta Q_{\text{fit}}(p) = \sum_{i=1}^{9} \left(a_i \cdot \Delta Q_i(p) \right), \tag{4}$$

where ΔQ_i and a_i are the anomalous heating rates and fitting coefficients respectively for each of the nine vertically localized forcings i. The a_i coefficients were calculated so as to minimize the least-squares difference between Q_{fit} and the global-mean heating profile of a chosen case, Q_{case} (Figure 3, left column). Best fits are expected to be unique given that the profiles of the vertically localized forcings are mostly nonoverlapping and hence mostly orthogonal.

The heating profiles for the realistic common forcings and atm_4 are very closely approximated by linearly combining the nine idealized vertically localized cases (Figure 3, left column). The only deviations occur above the tropopause for the $2 \times CO_2$ and 3%Sol cases where there is insufficient vertical resolution in the localized forcing experiments. For $2 \times CO_2$, we set the heating rate to zero above 150 hPa before fitting because the sharp "kink" around the tropopause (Figure S4) otherwise makes the fit inaccurate. Since the majority of the cloud-radiative effect comes from clouds in the tropopause, we expect excluding the stratosphere to make little difference.

The heating profiles for the common forcings (and atm_4) are very closely approximated by linearly combining the nine idealized vertically localized cases (Figure 3, left column). The only deviations occur above the tropopause for the $2 \times CO_2$ and 3%Sol cases where there is insufficient vertical resolution in the localized forcing experiments.

Using the same a_i coefficients obtained in Equation 4, we then estimate the globally averaged vertical profiles of change in temperature, RH, and cloud fraction (each denoted by X) in response to each vertically distributed forcing, whose instantaneous surface forcing is F_{sfc} thus:

$$\Delta X_{\text{fit}}(p) = \left(\frac{F_{\text{sfc}}}{4 \text{Wm}^{-2}} \cdot \Delta X_{\text{sfc\_4}} \right) + \sum_{i} \left(a_i \cdot \Delta X_i(p) \right). \tag{5}$$

The first term on the right-hand side accounts for contributions from surface forcing, using the results from a 4 W m^{-2} uniform surface heating experiment (sfc_4, see Table S2), appropriately weighted.

The linear combination of idealized vertically localized heating anomalies closely approximates the adjustments of temperature, RH, and cloud fraction diagnosed from the model (Figure 3). This suggests that the global-average vertical structure of these adjustments is primarily determined by the vertical profile of instantaneous heating anomalies.

The contributions to these profiles from the surface components of the forcings were found to be minor in general, consistent with our finding that the cloud adjustment to uniform surface-only forcing is very small.
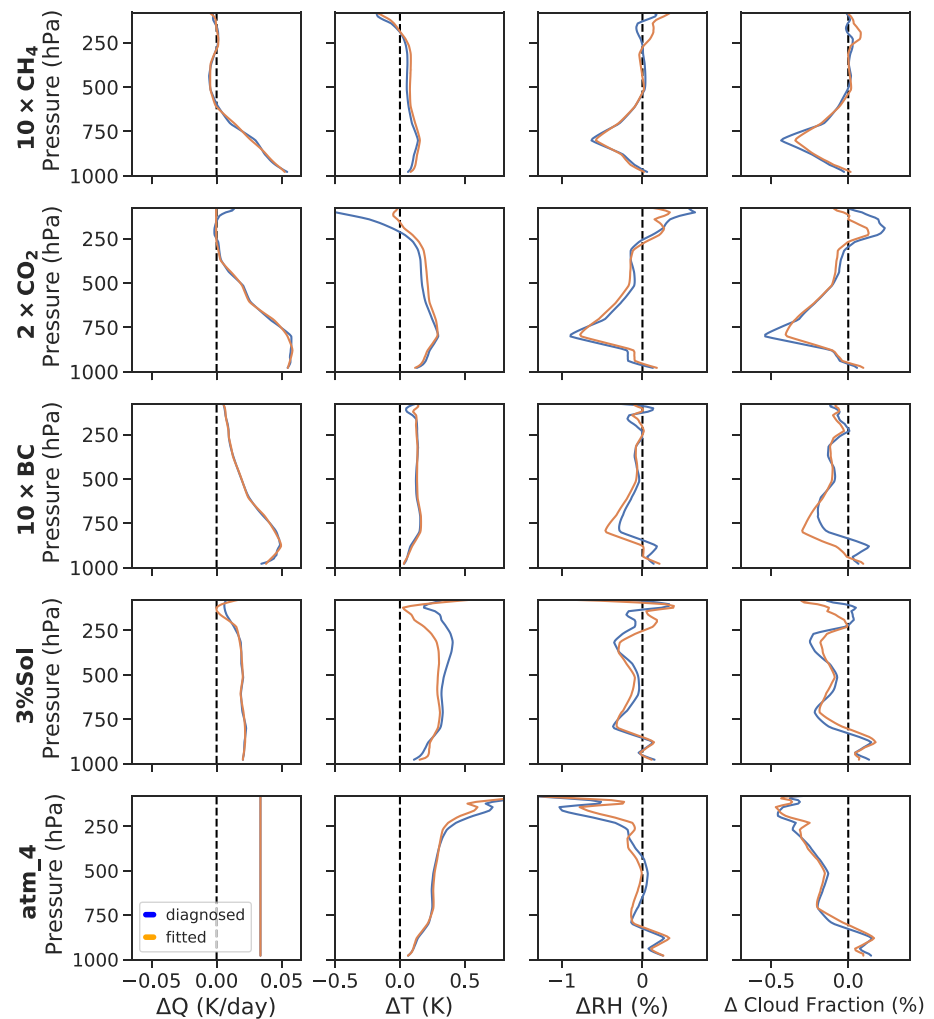
Figure 3. Global-mean vertical heating anomaly profiles (ΔQ) and rapid adjustments of temperature (ΔT), relative humidity (ΔRH) and cloud fraction. Shown are the results from the original cases (*blue*) and linear combinations of the results from the vertically localized forcing experiments (*orange*) including an appropriate surface term (Equation 5). Fitted heating rates are best fits to the original heating rates (Equation 4) in all cases (except for $2 \times CO_2$ where we set the stratospheric heating anomalies to zero before fitting). The orange lines for other variables are created from the fits of heating rates (Equation 5).

The notable exception to this was in the solar forcing case, where the majority of instantaneous forcing is from the surface component (4.88 W m^{-2}, compared to a 2.19 W m^{-2} atmospheric component), such that the surface component makes a nonnegligible contribution to the cloud fraction change profile (Figure S5).

Considering the global-average top-of-atmosphere cloud-radiative adjustments to forcings, we find that the linear combinations of vertically localized heating experiments generally predict the correct sign, and roughly the magnitude, of the vertically distributed forcings (Figure 4). The cloud-radiative adjustments to $10 \times BC$ are surprisingly well predicted, despite the cloud responses here being the least accurately predicted (although still captured to first order, Figure 3). This is possibly due to errors in the predicted cloud response fortuitously canceling out in some way (e.g., errors in the vertical may compensate for errors in the horizontal distribution). The largest errors are for CO_2 and CH_4, where the positive SW adjustments are considerably underestimated. Inspection of the cloud fraction profiles in Figure 3 suggests this may partly result from an underestimation of the lower-tropospheric cloud fraction decrease by the simple linear combination method, and potentially from differences in estimation of cloud changes near the tropopause. That the predicted net adjustments are more accurate than the individual SW and LW adjustments can be explained by
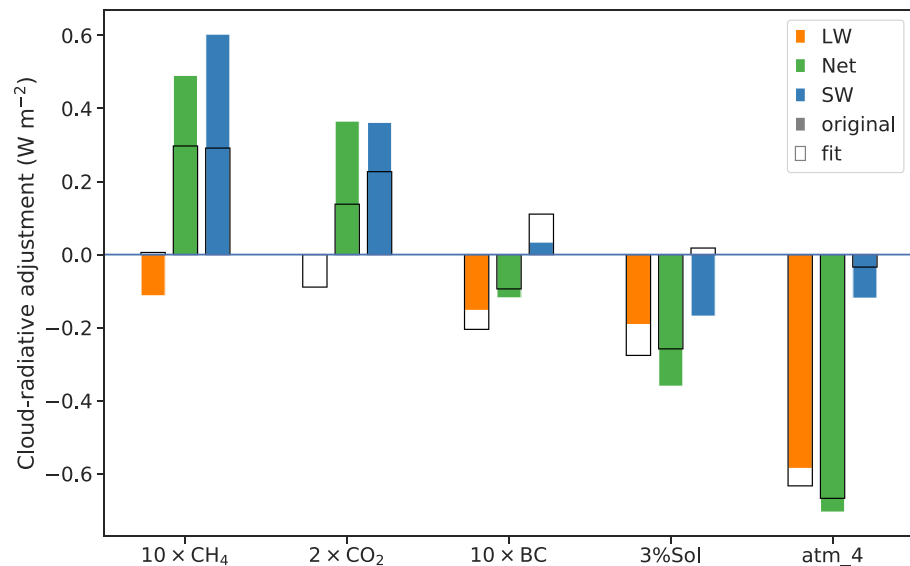
Figure 4. A comparison of the cloud-radiative adjustments predicted from linearly combining vertically localized forcing experiments (*empty bars*) versus the radiative adjustments calculated from the relevant experiments themselves (*solid bars*).

compensating errors in SW and LW. Errors in this approach may also result from the linear combination of cloud-radiative adjustments being unable to account for the nonlinear effects of cloud overlap.

The results in Figures 3 and 4 account for the finding of Figure 2c (filled symbols) that the sign and magnitude of cloud-radiative adjustments are mostly explained by the vertical structure of the instantaneous atmospheric forcing, as measured by the heating-weighted pressure centroid. Positive CRE adjustments result from the "bottom-heaviest" instantaneous atmospheric heating profiles of $2 \times CO_2$ and $10 \times CH_4$, negative CRE adjustments from 3%Sol and atm_4, whose instantaneous heating profiles are fairly uniform with altitude, while $10 \times BC$ is intermediate.

Although our interpretation is based on a single climate model, we note that the cloud-radiative adjustments in Figure 4 are reasonably representative of those simulated by a range of CMIP5 models (Figure 4 of Smith et al., 2018). In particular, models consistently simulate positive cloud-radiative adjustments to CO_2, and negative adjustments to solar forcing, in agreement with our results. Note that the results of Smith et al. (2018) use different magnitudes of the CH_4 and solar forcings, and include the stomatal conductance effect of $2 \times CO_2$. Increases to CO_2 lead to reduced to evapotranspiration and thus reduced low cloud over many highly forested areas for a positive effect on the cloud-radiative adjustment (Doutriaux-Boucher et al., 2009). We found that including this effect approximately doubles the cloud adjustment to $2 \times CO_2$ forcing in CAM4 (0.76 vs. 0.37 W m^{-2}; not shown).

5. Summary and Conclusions

We have demonstrated through a series of idealized experiments with vertically localized atmospheric heating that cloud-radiative adjustments are sensitive principally to the altitude of atmospheric heating caused instantaneously by the forcing agent. At levels where there is an instantaneous positive heating tendency, the air becomes warmer and drier and the cloud fraction decreases. However, heating at any level above the boundary layer stabilizes the troposphere below and suppresses vertical mixing, thus causing moistening and increased cloud fraction at lower levels. As the net result of these two effects, lower-tropospheric heating results in positive cloud-radiative adjustment (dominated by the SW effect of reduced low cloud fraction), while mid- and upper-tropospheric heating causes negative adjustment (due to the combined LW and SW effects of increased low cloud and reduced free-tropospheric cloud). For negative forcings, the signs of all effects are reversed and the magnitudes are similar.

We find that the global-mean cloud-radiative adjustments to common forcings can be reasonably well explained by linearly combining the idealized vertically localized forcings so as to fit the vertical heating profiles caused by the various forcing agents. In particular, our results suggest that positive cloud adjustment commonly-found in GCMs to the greenhouse gas forcing agents CO_2 and CH_4 is explained by their relatively bottom-heavy atmospheric heating profiles; by contrast, the negative cloud adjustment to solar forcing is caused by its relatively larger free-tropospheric heating. Our findings are consistent also with previous evidence that cloud-radiative adjustments depend on the altitude of absorbing aerosols such as black carbon (Allen et al., 2019; Samset & Myhre, 2015).

Although successful in explaining the sign and relative magnitude of adjustments for different agents, our method using global-mean vertical profiles does not give quantitatively accurate estimates. This may be for instance because of neglecting the geographical pattern and the seasonal cycle of the instantaneous heating, perhaps especially the contrast between its effects in cloudy and cloud-free air. Further investigation is needed of these aspects. With such refinement, we expect that this approach will provide a useful basis to interpret inter-model differences in cloud adjustments, to the extent that such differences result from uncertainties in the distribution of IRF.

Data Availability Statement

The data that support the findings of this study are available from https://doi.org/10.6084/m9.figshare.14386799.

References

Allen, R. J., Amiri-Farahani, A., Lamarque, J.-F., Smith, C., Shindell, D., Hassan, T., & Chung, C. E. (2019). Observationally constrained aerosol–cloud semi-direct effects. *npj Climate and Atmospheric Science*, *2*(1), 16. https://doi.org/10.1038/s41612-019-0073-9

Amiri-Farahani, A., Allen, R. J., Neubauer, D., & Lohmann, U. (2017). Impact of Saharan dust on North Atlantic marine stratocumulus clouds: Importance of the semidirect effect. *Atmospheric Chemistry and Physics*, *17*(10), 6305–6322. https://doi.org/10.5194/acp-17-6305-2017

Andrews, T., & Forster, P. M. (2008). CO_2 forcing induces semi-direct effects with consequences for climate feedback interpretations. *Geophysical Research Letters*, *35*(4). https://doi.org/10.1029/2007GL032273

Andrews, T., Gregory, J. M., Forster, P. M., & Webb, M. J. (2012). Cloud adjustment and its role in CO_2 radiative forcing and climate sensitivity: A review. *Surveys in Geophysics*, *33*(3), 619–635. https://doi.org/10.1007/s10712-011-9152-0

Ban-Weiss, G. A., Cao, L., Bala, G., & Caldeira, K. (2012). Dependence of climate forcing and response on the altitude of black carbon aerosols. *Climate Dynamics*, *38*(5), 897–911. https://doi.org/10.1007/s00382-011-1052-y

Bellouin, N., Quaas, J., Gryspeerdt, E., Kinne, S., Stier, P., Watson-Parris, D., et al. (2020). Bounding global aerosol radiative forcing of climate change. *Reviews of Geophysics*, *58*(1), e2019RG000660. https://doi.org/10.1029/2019RG000660

Beucler, T., Cronin, T., & Emanuel, K. (2018). A linear response framework for radiative-convective instability. *Journal of Advances in Modeling Earth Systems*, *10*(8), 1924–1951. https://doi.org/10.1029/2018ms001280

Ceppi, P., Brient, F., Zelinka, M. D., & Hartmann, D. L. (2017). Cloud feedback mechanisms and their representation in global climate models. *Wiley Interdisciplinary Reviews: Climate Change*, *8*(4), e465. https://doi.org/10.1002/wcc.465

Chung, E.-S., & Soden, B. J. (2015). An assessment of direct radiative forcing, radiative adjustments, and radiative feedbacks in coupled ocean–atmosphere models. *Journal of Climate*, *28*(10), 4152–4170. https://doi.org/10.1175/jcli-d-14-00436.1

Colman, R. A., & McAvaney, B. J. (2011). On tropospheric adjustment to forcing and climate feedbacks. *Climate Dynamics*, *36*(9), 1649–1658. https://doi.org/10.1007/s00382-011-1067-4

Conley, A. J., Lamarque, J.-F., Vitt, F., Collins, W. D., & Kiehl, J. (2013). PORT, a CESM tool for the diagnosis of radiative forcing. *Geoscientific Model Development*, *6*(2), 469–476. https://doi.org/10.5194/gmd-6-469-2013

Dinh, T., & Fueglistaler, S. (2017). Mechanism of fast atmospheric energetic equilibration following radiative forcing by CO_2. *Journal of Advances in Modeling Earth Systems*, *9*(7), 2468–2482. https://doi.org/10.1002/2017ms001116

Dong, Y., Proistosescu, C., Armour, K. C., & Battisti, D. S. (2019). Attributing historical and future evolution of radiative feedbacks to regional warming patterns using a Green's function approach: The preeminence of the western Pacific. *Journal of Climate*, *32*(17), 5471–5491. https://doi.org/10.1175/JCLI-D-18-0843.1

Doutriaux-Boucher, M., Webb, M. J., Gregory, J. M., & Boucher, O. (2009). Carbon dioxide induced stomatal closure increases radiative forcing via a rapid reduction in low cloud. *Geophysical Research Letters*, *36*(2). https://doi.org/10.1029/2008gl036273

Forster, P. M., Richardson, T., Maycock, A. C., Smith, C. J., Samset, B. H., Myhre, G., et al. (2016). Recommendations for diagnosing effective radiative forcing from climate models for CMIP6. *Journal of Geophysical Research: Atmospheres*, *121*(20), 12460–12475. https://doi.org/10.1002/2016jd025320

Gregory, J., & Webb, M. (2008). Tropospheric adjustment induces a cloud component in CO_2 forcing. *Journal of Climate*, *21*(1), 58–71. https://doi.org/10.1175/2007JCLI1834.1

Hansen, J., Sato, M., & Ruedy, R. (1997). Radiative forcing and climate response. *Journal of Geophysical Research*, *102*(D6), 6831–6864. https://doi.org/10.1029/96jd03436

Hartmann, D. L. (1994). *Global physical climatology*. Academic Press.

Kamae, Y., Chadwick, R., Ackerley, D., Ringer, M., & Ogura, T. (2019). Seasonally variant low cloud adjustment over cool oceans. *Climate Dynamics*, *52*(9–10), 5801–5817. https://doi.org/10.1007/s00382-018-4478-7

Kamae, Y., & Watanabe, M. (2012). On the robustness of tropospheric adjustment in CMIP5 models. *Geophysical Research Letters*, *39*(23). https://doi.org/10.1029/2012GL054275

Kamae, Y., & Watanabe, M. (2013). Tropospheric adjustment to increasing CO_2: Its timescale and the role of land–sea contrast. *Climate Dynamics*, *41*(11–12), 3007–3024. https://doi.org/10.1007/s00382-012-1555-1

Kamae, Y., Watanabe, M., Ogura, T., Yoshimori, M., & Shiogama, H. (2015). Rapid adjustments of cloud and hydrological cycle to increasing CO_2: A review. *Current Climate Change Reports*, *1*(2), 103–113. https://doi.org/10.1007/s40641-015-0007-5

Klein, S. A., & Hartmann, D. L. (1993). The seasonal cycle of low stratiform clouds. *Journal of Climate*, *6*(8), 1587–1606. https://doi.org/10.1175/1520-0442(1993)006<1587:tscols>2.0.co;2

Koch, D., & Del Genio, A. D. (2010). Black carbon semi-direct effects on cloud cover: Review and synthesis. *Atmospheric Chemistry and Physics*, *10*(16), 7685–7696. https://doi.org/10.5194/acp-10-7685-2010

Kuang, Z. (2010). Linear response functions of a cumulus ensemble to temperature and moisture perturbations and implications for the dynamics of convectively coupled waves. *Journal of the Atmospheric Sciences*, *67*(4), 941–962. https://doi.org/10.1175/2009JAS3260.1

Myhre, G., Forster, P. M., Samset, B. H., Hodnebrog, O., Sillmann, J., Aalbergsjø, S. G., et al. (2017). PDRMIP: A precipitation driver and response model intercomparison project-protocol and preliminary results. *Bulletin of the American Meteorological Society*, *98*(6), 1185–1198. https://doi.org/10.1175/bams-d-16-0019.1

Myhre, G., Shindell, D., Bréon, F.-M., Collins, W., Fuglestvedt, J., Huang, J., et al. (2014). *Anthropogenic and natural radiative forcing* (Technical report AR5). In *Climate change 2013: The physical science basis. Contribution of working group I to the fifth assessment report of the intergovernmental panel on climate change*. Cambridge University Press. Retrieved from https://www.ipcc.ch/report/ar5/wg1/

Neale, R. B., Richter, J. H., Conley, A. J., Park, S., Lauritzen, P. H., Gettelman, A., et al. (2010). *Description of the NCAR Community Atmosphere Model (CAM 4.0)*.

Richardson, T. B., Forster, P. M., Smith, C. J., Maycock, A. C., Wood, T., Andrews, T., et al. (2019). Efficacy of climate forcings in PDRMIP models. *Journal of Geophysical Research: Atmospheres*, *124*(23), 12824–12844. https://doi.org/10.1029/2019jd030581

Samset, B. H., & Myhre, G. (2015). Climate response to externally mixed black carbon as a function of altitude. *Journal of Geophysical Research: Atmospheres*, *120*(7), 2913–2927. https://doi.org/10.1002/2014jd022849

Sand, M., Samset, B. H., Tsigaridis, K., Bauer, S. E., & Myhre, G. (2020). Black carbon and precipitation: An energetics perspective. *Journal of Geophysical Research: Atmospheres*, *125*(13), e2019JD032239. https://doi.org/10.1029/2019JD032239

Sherwood, S. C., Bony, S., Boucher, O., Bretherton, C., Forster, P. M., Gregory, J. M., & Stevens, B. (2015). Adjustments in the forcing-feedback framework for understanding climate change. *Bulletin of the American Meteorological Society*, *96*(2), 217–228. https://doi.org/10.1175/BAMS-D-13-00167.1

Shine, K., Fouquart, Y., Ramaswamy, V., Solomon, S., & Srinivasan, J. (1995). Radiative forcing (Technical report). In *IPCC report on radiative forcing of climate change and an evaluation of the IPCC IS92 emission scenarios*. Retrieved from https://www.ipcc.ch/report/climate-change-1994-radiative-forcing-of-climate-change-and-an-evaluation-of-the-ipcc-is92-emission-scenarios-2/

Shine, K. P., Cook, J., Highwood, E. J., & Joshi, M. M. (2003). An alternative to radiative forcing for estimating the relative importance of climate change mechanisms. *Geophysical Research Letters*, *30*(20). https://doi.org/10.1029/2003GL018141

Smith, C. J., Kramer, R. J., Myhre, G., Alterskjær, K., Collins, W., Sima, A., et al. (2020). Effective radiative forcing and adjustments in CMIP6 models (preprint). *Atmospheric Chemistry and Physics*. https://doi.org/10.5194/acp-2019-1212

Smith, C. J., Kramer, R. J., Myhre, G., Forster, P. M., Soden, B. J., Andrews, T., et al. (2018). Understanding rapid adjustments to diverse forcing agents. *Geophysical Research Letters*, *45*(21), 12023–12031. https://doi.org/10.1029/2018gl079826

Stjern, C. W., Samset, B. H., Boucher, O., Iversen, T., Lamarque, J.-F., Myhre, G., et al. (2020). How aerosols and greenhouse gases influence the diurnal temperature range. *Atmospheric Chemistry and Physics*, *20*(21), 13467–13480. https://doi.org/10.5194/acp-20-13467-2020

Swales, D. J., Pincus, R., & Bodas-Salcedo, A. (2018). The cloud feedback model intercomparison project observational simulator package: Version 2. *Geoscientific Model Development*, *11*(1), 77–81. https://doi.org/10.5194/gmd-11-77-2018

Zelinka, M. D., Klein, S. A., & Hartmann, D. L. (2012). Computing and partitioning cloud feedbacks using cloud property histograms. Part II: Attribution to changes in cloud amount, altitude, and optical depth. *Journal of Climate*, *25*(11), 3736–3754. https://doi.org/10.1175/JCLI-D-11-00249.1

Zelinka, M. D., Klein, S. A., Taylor, K. E., Andrews, T., Webb, M. J., Gregory, J. M., & Forster, P. M. (2013). Contributions of different cloud types to feedbacks and rapid adjustments in CMIP5. *Journal of Climate*, *26*(14), 5007–5027. https://doi.org/10.1175/jcli-d-12-00555.1

Zhou, C., Zelinka, M. D., & Klein, S. A. (2017). Analyzing the dependence of global cloud feedback on the spatial pattern of sea surface temperature change with a Green's function approach. *Journal of Advances in Modeling Earth Systems*, *9*(5), 2174–2189. https://doi.org/10.1002/2017MS001096